PAPER

Check for updates

Effect of doping mediated oxygen vacancies on the charge transfer ability of zinc oxide nanosheets for electrochemical glucose sensing†

Saptaka Baruah,[a] Bidyarani Maibam,[a] Jyoti Jaiswal,[a]
Ankit Kumar[b] and Sanjeev Kumar [ID] *[a]

We reported on hydrothermally synthesized zinc oxide (ZnO) nanosheets modified by doping with silver (Ag: 1, 2, 3, 4, and 5%) to improve their electrochemical properties for glucose sensing with and without an enzyme. SEM, XRD, EDX, and FTIR were used to investigate the microstructural, chemical, and optical properties of pristine ZnO and Ag-doped ZnO. XPS confirms that silver acts as an effective oxygen vacancy suppressor. Cyclic voltammetry studies revealed that the 5% Ag-doped ZnO electrode has a higher anodic current than the pristine ZnO and Ag (1, 2, 3, 4%)-doped ZnO electrodes. Because of the higher anodic current, the 5% Ag-doped ZnO electrode was used for sensing glucose with and without an enzyme. The 5% Ag-doped ZnO nanosheet-based electrode without an enzyme exhibited enhanced sensitivity ($\sim$104.7 μA mM^{-1} cm^{-2}), lower detection limits ($\sim$0.06 mM), higher selectivity, practical repeatability & reproducibility, and good stability compared to the 5% Ag-doped ZnO nanosheet-based electrode with an enzyme (sensitivity $\sim$98.3 μA mM^{-1} cm^{-2} and LOD $\sim$0.098 mM), with each having a response time of $\sim$5 s.

1. Introduction

Increased sugar consumption in the diet has been linked to a number of serious illnesses, such as cardiovascular diseases (*e.g.*: stroke or heart attack, heart failure), sleep apnea, type 2 diabetes, metabolic syndrome, and obesity.[1,2] Diabetes is a metabolic condition that results in an elevated blood sugar level, which triggers multiple metabolic pathways linked to inflammation and apoptosis.[3] There is currently no cure for this disease, so diabetic individuals must constantly monitor their blood glucose level in order to avoid health problems. As a result, a biosensor that can detect glucose quickly, accurately, and consistently is required.[4] In this regard, surface plasmon resonance (SPR), fluorescence, colorimetric, and surface enhanced Raman spectroscopy (SERS) technique-based sensors have gained appreciable attention for glucose detection.[5] For example, Hu *et al.*[5] recently reported a cost-effective cadmium telluride (CdTe) quantum dot (QD) based visual sensor for glucose detection (limit of detection (LOD) $\sim$

5 nm) based on a colorimetric technique. A nanoceria-based glucose sensor was reported by Liu *et al.*[6] based on a fluorescence technique. The sensor exhibits a lower LOD of $\sim$8.9 μM in buffer. He *et al.*[7] reported a sensitive optical sensor for glucose monitoring using Ag/Au bimetallic nanoshells, which detected 4.4 $\pm$ 0.4 $\times$ 10^{-3} M glucose in a serum sample. Interestingly, there has been a significant shift in glucose detection using electrochemical techniques, which are efficient and flexible methods for enabling real-time and on-site measurement in different fields. So, in recent times, electrochemical glucose sensors have attracted lots of attention due to their low cost, simple fabrication technique, high accuracy, selectivity and sensitivity.[8] It is well known that the typical blood glucose concentration range in the human body is 110 $\pm$ 25 mg dl^{-1} (approximately 4.7–7.5 mM). However, diabetes patients have substantially higher blood glucose concentrations ($>$20 mM).[9] Most glucose biosensors need to use enzymes to improve sensitivity and selectivity when measuring blood glucose levels. The literature suggests that glucose oxidase (GOx) is a promising enzyme for the detection of glucose due to its higher selectivity towards glucose.[10–12] However, the activity of enzyme immobilized glucose sensors has limitations, like poor long-term stability and reproducibility. Further, GOx is vulnerable to a variety of experimental conditions such as humidity, temperature, pH, ionic detergents, and hazardous compounds. Consequently, a non-enzymatic glucose biosensor that is highly sensitive and

[a] Centre for Advanced Research, Department of Physics, Rajiv Gandhi University, Arunachal Pradesh-791112, India. E-mail: sanjeev.kumar@rgu.ac.in, sanjeev.dr@gmail.com
[b] Department of Mechanical & Industrial Engineering (MIED), IIT Roorkee, Roorkee 247667, India

selective and can be made at a low cost is required.[13] Many transition metal oxides including CuO, NiO, ZnO, Co_3O_4, and MnO_2 have recently made significant contributions to non-enzymatic sensors.[14,15] Among these, ZnO has several unique features such as a wide band gap, excellent chemical characteristics, superior biocompatibility,[16] high isoelectric point (IEP),[17] non-toxicity,[18] fast electron transfer capability,[16,19] *etc.*, along with optical,[17,20] electrical[21] and piezoelectric[22] and pyroelectric[23] properties. In spite of all these properties, the sensing properties of pristine ZnO are found to be inadequate. Earlier studies state that modifying ZnO by either doping or functionalizing catalysts, such as noble metals, transition metals, carbon nanotubes, graphene, *etc.*, with unique nanostructures could alleviate this problem and thus improve biosensor performances.[24–31] For example, Raza *et al.* reported a non-enzymatic glucose sensor screen printed electrode based on Fe-doped zinc oxide (Fe@ZnO) nanoparticles synthesized by a simple stirring method, which showed a good LOD of 0.30 μM.[25] Luo *et al.* described the development of a high-performance (sensitivity of 7.184 MHz mM^{-1}) Mn-doped ZnO multilayer structure Love mode surface acoustic wave (SAW) biosensor for continuous glucose monitoring.[26] Shukla *et al.* also synthesized Mn-doped ZnO nanopencils for an enzymatic glucose biosensor and found a 17-fold increase in sensitivity for Mn-doped ZnO in comparison to pristine ZnO.[27] Ghosh *et al.* reported an Al-doped ZnO thin film for label-free glucose detection based on fluorescence quenching which has a very high sensitivity with a LOD of 20 μM.[28] Vijayaprasath *et al.* studied the glucose-sensing behavior of Co-doped ZnO nanoparticles made by co-precipitation and found that the constructed biosensor is extremely selective towards glucose.[29] In addition, Mahmoud *et al.* developed an impedimetric non-enzymatic sensor based on Cu-doped ZnO nanoparticles, which exhibited a greater sensitivity with a good LOD in comparison to pristine ZnO.[30] Peng *et al.*[31] reported a non-enzymatic glucose sensor based on Ga-doped ZnO nanorods, which exhibited a sensitivity of 33.4 μA mM^{-1} cm^{-2} with good stability and excellent anti-interference ability. Chakraborty *et al.*[32] developed C-doped ZnO nanorod arrays for non-enzymatic glucose sensing which showed a sensitivity of 13.66 μA mM^{-1} cm^{-2} with a linear range of 0.7–14 mM. The literature suggests that there are several reports available regarding transition metal doped ZnO for applications in glucose sensing, but few are reported for noble metals. Ag is a noble metal with strong electrical conductivity and chemical stability.[33] Ag-doped ZnO can be easily synthesized under simple circumstances and has already been used to prevent the recombination of photo-induced electron–hole pairs in photo-degradation reactors and dye-sensitized solar cells.[34,35] Therefore, doping ZnO with Ag has the potential to boost the transfer of redox electrons from ZnO to the electrode of a glucose sensor.[36] A Ag-doped ZnO nanorod-based enzymatic glucose sensor has been reported by Fan Zhou *et al.*,[36] which showed a sensitivity of 3.85 μA mM^{-1} cm^{-2} with a detection limit of 1.5 μM. Further, newly developed morphologies (*e.g.*, nanorings, nanocombs,

nanoflakes, nanorods, nanobelts, nanoworms, thin films, *etc.*) are beneficial for sensing applications because of their larger specific surface areas and surface activities.[37–46] To date, great initiatives have been taken to create an exceptional ZnO nanostructure that maximizes the number of exposed sites. There are several techniques, such as chemical vapour deposition, spray pyrolysis, sol–gel methods, hydrothermal methods, *etc.*, available for synthesizing such ZnO nanostructures.[47–49] Among them, the hydrothermal process has attracted many researchers due to its specific characteristics, such as simple equipment, environment friendliness, moderate preparation conditions, and low cost.[50] Here, we aimed to fabricate ZnO with a unique nanostructure through a hydrothermal method and to improve its properties with Ag doping for electrochemical glucose sensing. Besides, several standard characterization techniques have been performed to show and determine the microstructural, surface, and electrochemical properties of the prepared pristine and Ag-doped ZnO matrices. Our findings manifest that (i) the hydrothermally synthesized pristine ZnO has a nanosheet-like structure and with an increase in Ag doping concentration, the size of the prepared ZnO nanosheets decreases; (ii) the charge transfer characteristics have been enhanced for Ag-doped ZnO samples, and (iii) a non-enzymatic electrode based on the Ag-doped ZnO nanosheets has good glucose sensing performance (sensitivity ~104.7 μA mM^{-1} cm^{-2}) compared to a prepared enzymatic electrode (sensitivity ~98.3 μA mM^{-1} cm^{-2}).

2. Experimental

2.1 Materials and methods

Zinc nitrate hexahydrate ($Zn(NO_3)_2 \cdot 6H_2O$) (Merck), glucose oxidase (GOx) (*Aspergillus niger* RM7064-10000U), phosphate buffered saline (PBS) (0.01 M, pH 7.4) (HIMEDIA), potassium ferrocyanide trihydrate ($K_4[Fe(CN)_6] \cdot 3H_2O$) (Merck), potassium ferricyanide ($K_3[Fe(CN)_6]$) (Merck), sodium hydroxide pellets (NaOH) (Merck), silver nitrate ($AgNO_3$) (Merck), potassium bromide (KBr) (Merck), uric acid ($C_5H_4N_4O_3$) (Loba Chemie), ascorbic acid ($C_6H_8O_6$) (Merck), cholesterol ($C_{27}H_{46}O$) (SRL) and methanol (CH_3OH) (Merck) were purchased from Zenith India. Anhydrous D-(+)-glucose ($C_6H_{12}O_6$) (Merck) was purchased from North-East Chemical Corporation, India.

The surface morphological and structural properties of the pristine and Ag-doped ZnO samples were investigated using a field emission scanning electron microscope (FESEM, Ultra plus Carl Zeiss) and an X-ray diffractometer (XRD, D8 Advance Eco-Bruker), respectively. Furthermore, energy dispersive X-ray spectroscopy (EDX, Oxford Instruments), attached to the FESEM, was used to determine the elemental composition of the samples. X-ray photoelectron spectroscopy (XPS, PHI Versa Probe III electron spectrometer) was used to determine the chemical states of the pristine and Ag-doped ZnO samples. The Fourier transform infrared

(FTIR) spectra of the samples were recorded using an FTIR spectrometer (Thermo Scientific Nicolet iS5) with KBr pellets.

The electrochemical characteristics of the prepared electrodes were studied and glucose-sensing measurements were performed by using an electrochemical workstation (Gamry Reference 3000) at room temperature with a three-electrode system in 0.01 M PBS (pH 7.4) solution containing 5 mM $[Fe(CN)_6]^{3-/4-}$. In the electrochemical workstation, the prepared electrodes, a Pt wire, and Ag/AgCl with a saturated KCl solution were used as a working electrode, a counter electrode, and a reference electrode, respectively. The electron transfer properties between the electrode surface and electrolyte were investigated with electrochemical impedance spectroscopy (EIS) using an alternating voltage of 10 mV with a frequency ranging from 0.2 Hz to 100 kHz. Cyclic voltammetry was used to explore the electrochemical characteristics of the prepared electrodes, along with quantifying the glucose concentration in the sample solution. The anti-interference ability and effect of temperature on the prepared electrodes were studied using square wave voltammetry (SWV).

2.2 Fabrication of electrodes

In this work, pristine ZnO, 1% Ag-doped ZnO (ZnO:Ag1), 2% Ag-doped ZnO (ZnO:Ag2), 3% Ag-doped ZnO (ZnO:Ag3), 4% Ag-doped ZnO (ZnO:Ag4) and 5% Ag-doped ZnO (ZnO:Ag5) were synthesized using a hydrothermal method (ESI,† section S1.1). As shown in Fig. 1, for the application of nonenzymatic and enzymatic glucose sensors, pristine and Ag-doped ZnO nanosheet based sensing electrodes were fabricated on ITO (indium tin oxide) coated glass substrates without and with glucose

oxidase (GOx) enzyme immobilization on the surface of the prepared nanosheets, respectively (ESI,† sections S1.2 and S1.3).

3. Material characterization and analysis

In this work, field emission scanning electron microscopy (FESEM), X-ray diffraction (XRD), X-ray photoelectron spectroscopy (XPS), energy dispersive X-ray spectroscopy (EDX), and Fourier transform infrared (FTIR) spectroscopy were used to investigate the microstructural, chemical, and surface properties of pristine ZnO and Ag-doped ZnO nanosheets. As shown in Fig. 2(a–f), the FESEM images display the growth of nanosheet-like structures for all the prepared pristine ZnO and Ag-doped ZnO samples (ESI,† section S2.1).

The crystal structure of the pristine and Ag-doped ZnO nanosheets was studied by the X-ray diffraction (XRD) technique. XRD patterns of the pristine and Ag-doped ZnO samples are displayed in Fig. 3. The X-ray diffractogram of pristine ZnO demonstrated multiple diffraction peaks at $2\theta \sim$ 31.74°, 34.41°, 36.24°, 47.53°, 56.56°, and 62.83° corresponding to the crystallographic planes (100), (002), (101), (102), (110), and (103), respectively, signifying the formation of a hexagonal wurtzite structure.[51] Also, the XRD diffractogram of Ag-doped ZnO nanosheets revealed additional diffraction peaks of the (111), (200), and (220) planes (marked with "*" in Fig. 3), matching with the face-centered-cubic (fcc) phase of metallic Ag,[52] which indicates the formation of crystalline silver clusters in the Ag-doped ZnO.[53] In addition, a small shift in XRD peak position towards a higher angle for ZnO:Ag1, ZnO:Ag2, and ZnO:Ag5
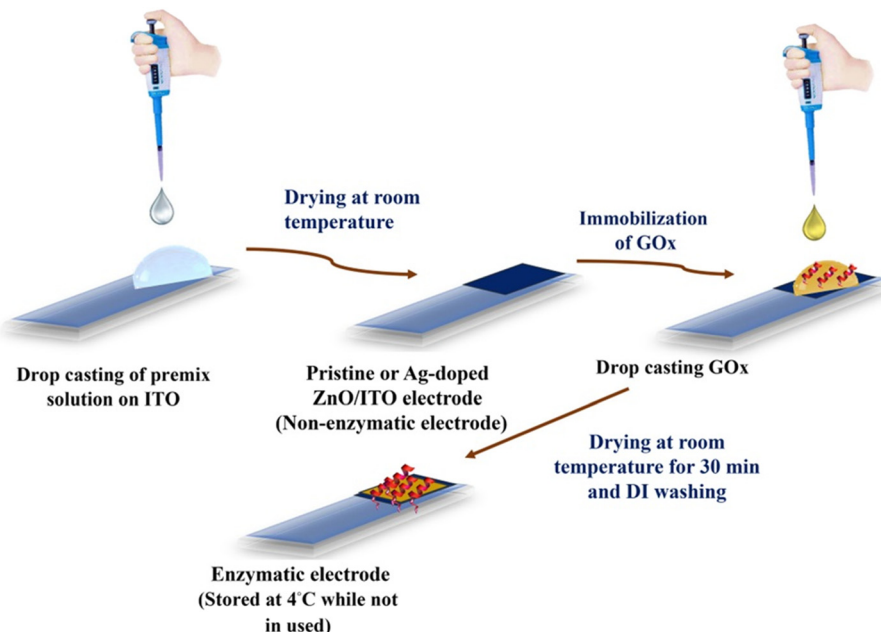

Fig. 1 Sequential schematic diagram to fabricate enzymatic and non-enzymatic electrodes for glucose sensing.
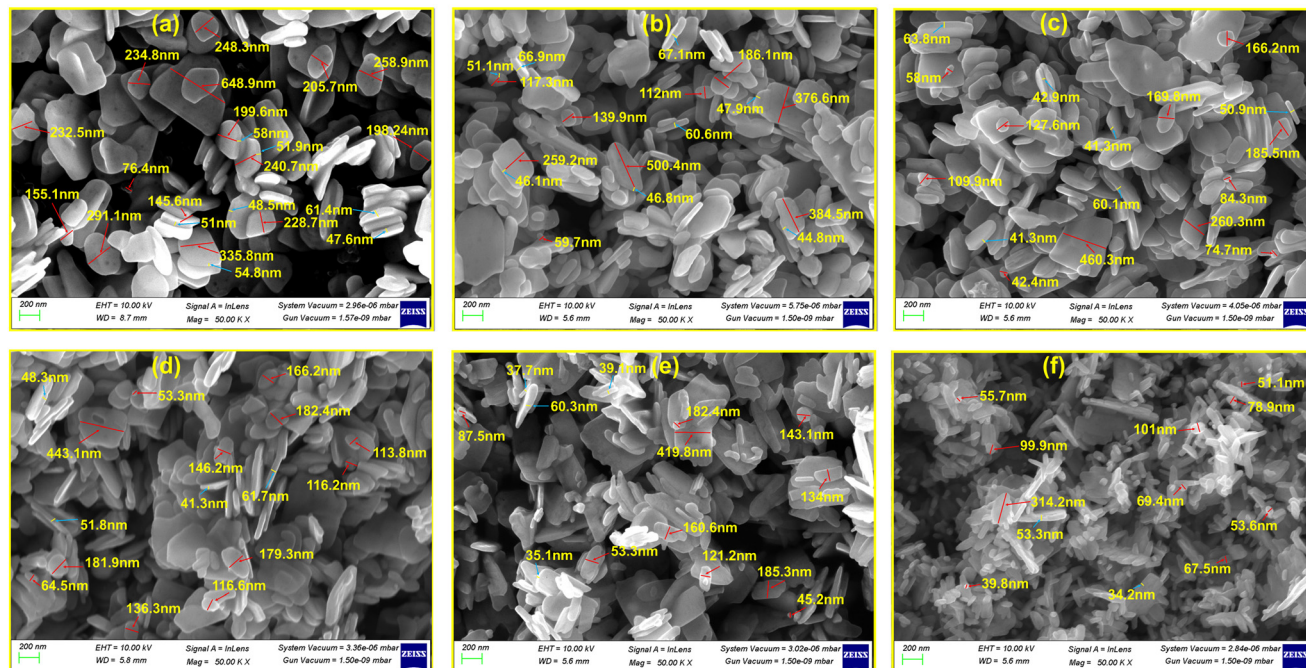
Fig. 2 FESEM micrographs of the pristine-ZnO (a), ZnO:Ag1 (b), ZnO:Ag2 (c), ZnO:Ag3 (d), ZnO:Ag4 (e), and ZnO:Ag5 (f) nanosheets.

was observed compared to that for ZnO:Ag3 and ZnO:Ag4. The observed shift in XRD peak position towards a higher angle for ZnO:Ag1, ZnO:Ag2, and ZnO:Ag5 suggests that Ag ions occupied the interstitial sites of ZnO.[54] However, the absence of such a shift in XRD peaks indicates the segregation of Ag particles over the grain boundaries of ZnO or incorporation of only a modest quantity of Ag ions in the substitutional Zn^{2+} sites. Due to the difference in ionic radii between Zn^{2+} and Ag^+, the Ag particles preferentially segregate near the ZnO grain boundaries, making the latter implausible.[54,55]

Further, the XPS survey scans of the pristine ZnO and ZnO:Ag5 nanosheets are displayed in Fig. S2 (ESI†). The

survey scan of pristine ZnO revealed characteristic peaks corresponding to C1s, Zn2p and O1s, which indicates the formation of ZnO. The survey scan of ZnO:Ag5 (Fig. S2†) demonstrated characteristic peaks corresponding to C1s, Zn2p, O1s, and Ag3d, indicating the successful incorporation of Ag ions in ZnO:Ag5. The presence of carbon in the samples is most likely due to the carbon adsorption process under ambient conditions. Here, the measured XPS data were calibrated with respect to the adventitious carbon C1s peak (284.8 eV).[56] Fig. 4(a) shows the high-resolution XPS (HRXPS) spectra of Zn2p for
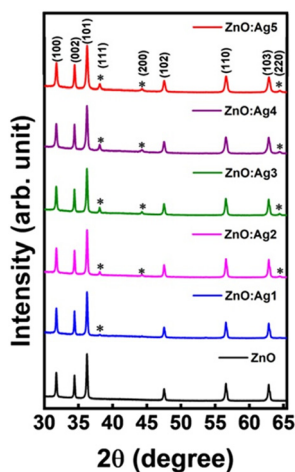

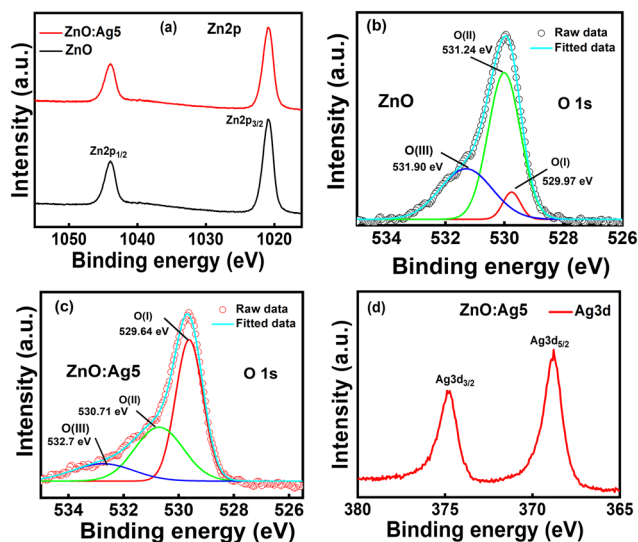**Fig. 3** The XRD diffractograms of pristine and (1–5%) Ag-doped ZnO nanosheets.

Fig. 4 HRXPS spectra of Zn2p (a), O1s (b and c), and Ag3d (d) for the pristine-ZnO and ZnO:Ag5 nanosheets.
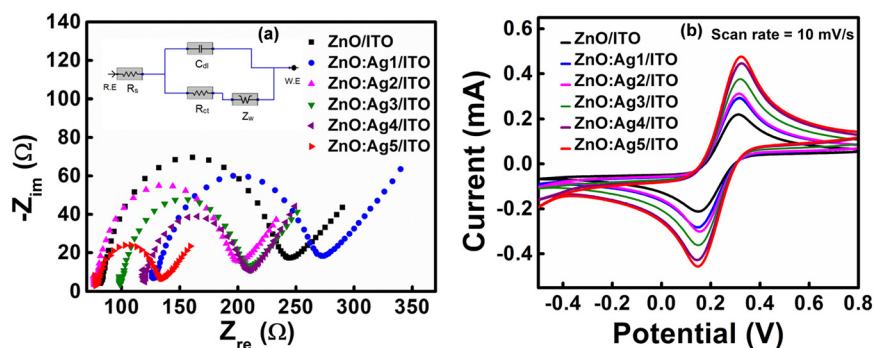
Fig. 5 (a) Nyquist plots for the pristine and Ag-doped ZnO/ITO electrodes, and Randles circuit (corresponding inset). (b) Cyclic voltammograms (CVs) obtained for pristine and Ag-doped ZnO/ITO electrodes at a scan rate of 10 mV s^{-1}.

pristine ZnO and ZnO:Ag5 nanosheets, where the Zn2p peak splits into Zn2p$_{3/2}$ and Zn2p$_{1/2}$ due to spin–orbit interaction with a doublet peak energy separation of around 23.0 eV,[57] confirming the Zn^{2+} state in the ZnO lattice.[58] For pristine ZnO, the split Zn2p peaks were found at ~1021.15 eV (Zn2p$_{3/2}$) and ~1044.15 eV (Zn2p$_{1/2}$). These values vary from those of stoichiometric ZnO (1022.1 eV for Zn2p$_{3/2}$ and 1045.1 eV for Zn2p$_{1/2}$), which can be ascribed to the charge transfer variation from Zn^{2+} to O^{2-} due to the presence of vacancies.[59] However, for the ZnO:Ag5 sample, the Zn2p$_{3/2}$ (~1020.92 eV) and Zn2p$_{1/2}$ (~1043.92 eV) peaks were found to shift slightly towards a lower binding energy, suggesting the presence of oxygen vacancies.[59] Fig. 4(b) and (c) show the

HRXPS spectra for the O1s core level of pristine ZnO and ZnO:Ag5 nanosheets, respectively. The deconvoluted peaks for pristine ZnO (Fig. 4(b)) were located at binding energies of ~529.97 eV, ~531.24 eV, and ~531.90 eV, corresponding to O(I), O(II), and O(III), respectively. The lower binding energy peak O(I) centered at ~529.97 eV is due to lattice oxygen (O$_L$), which contributes to the ZnO lattice's perfect hexagonal wurtzite structure.[60,61] The middle peak O(II) at a binding energy position of ~531.24 eV is attributed to the presence of oxygen vacancies (V$_{os}$) in the ZnO lattice.[61,62] The higher binding energy peak O(III) centered at ~531.90 eV is ascribed to chemisorbed oxygen species, such as OH$^-$ and –CO$_3$, and adsorbed H$_2$O.[63] In addition, the O1s spectrum is also shifted
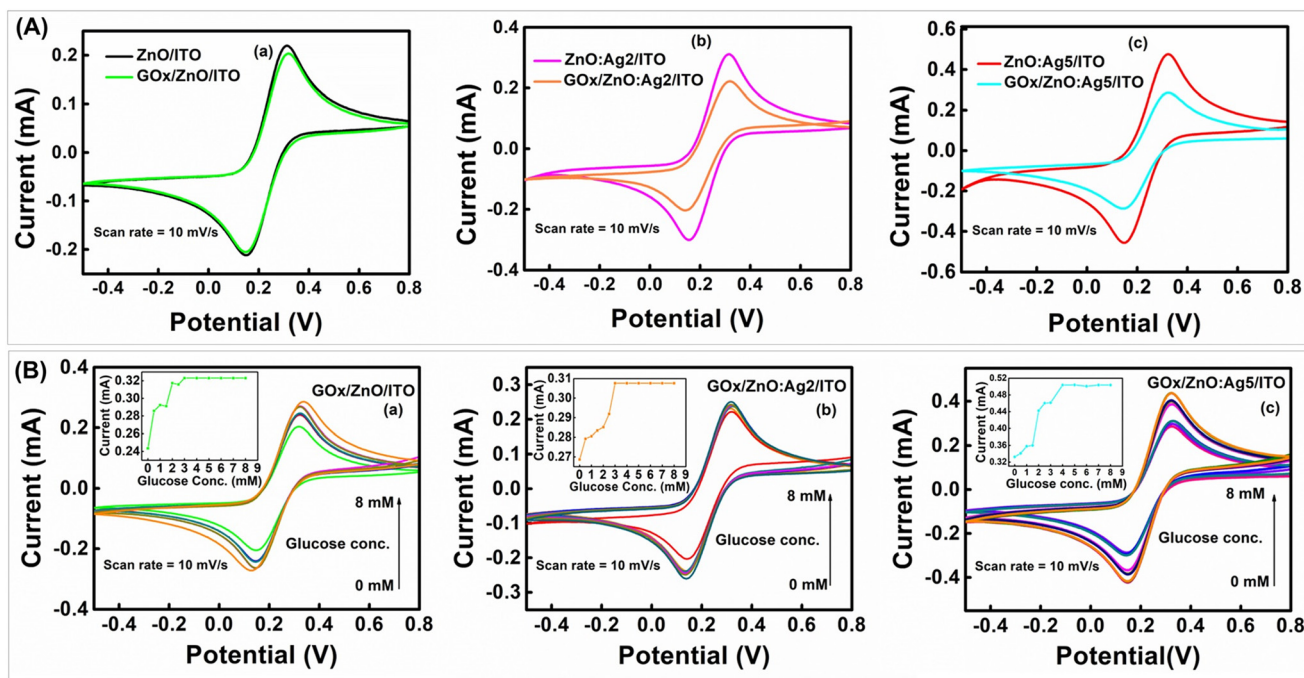

Fig. 6 (A) CVs obtained for (a) ZnO/ITO and GOx/ZnO/ITO electrodes, (b) ZnO:Ag2/ITO and GOx/ZnO:Ag2/ITO, and (c) ZnO:Ag5/ITO and GOx/ZnO:Ag5/ITO electrodes at a scan rate of 10 mV s^{-1}. (B) CVs of the prepared enzymatic sensing electrodes (a) GOx/ZnO/ITO, (b) GOx/ZnO:Ag2/ITO, (c) and GOx/ZnO:Ag5/ITO in the presence of 0–8 mM glucose at a scan rate of 10 mV s^{-1}. The corresponding insets show the current variation obtained as a function of glucose concentration.
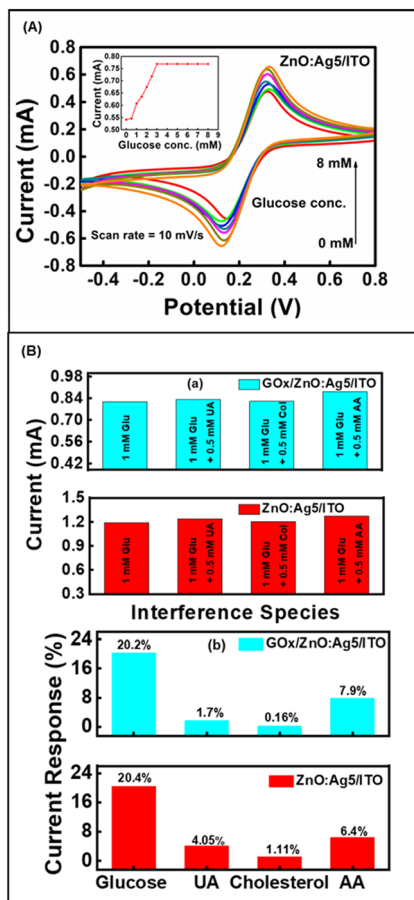
Fig. 7 (A) CVs of non-enzymatic (ZnO:Ag5/ITO) sensing electrode in the presence of 0–8 mM glucose concentration at a scan rate of 10 mV s^{-1}. The inset shows the current variation obtained as a function of glucose concentration. (B) (a) and (b) Effect of interfering species with 0.5 mM UA, cholesterol (Chol.), and AA each added to 1 mM glucose on the enzymatic (GOx/ZnO:Ag5/ITO) and non-enzymatic (ZnO:Ag5/ITO) electrodes.

towards lower binding energy for ZnO:Ag5 (Fig. 4(c)), which again confirms the presence of oxygen vacancies caused by Ag doping.[49] In order to assess the relative amounts of oxygen vacancies, the ratios of the respective O(II)/[O(I) + O(II)] sub-peak areas are determined, as listed in Table S1 (ESI†). Because of the strong binding energies between silver and oxygen, the ratio of O(II)/[O(I) + O(II)] drops for ZnO:Ag5, indicating that silver acts as an effective oxygen vacancy suppressor,[46] which is also corroborated by measured EDX results (ESI,† section S2.1). As can be seen from the HRXPS spectrum for Ag3d of ZnO:Ag5 (Fig. 4(d)), the difference between the peaks of Ag3d$_{5/2}$ (368.81 eV) and Ag3d$_{3/2}$ (374.81 eV) is 6.0 eV, confirming the presence of the purely metallic Ag state in ZnO:Ag5.[64–67] Moreover, the FTIR spectra (Fig. S3†) confirmed the formation of pristine ZnO and the successful incorporation of Ag ions into the ZnO host matrix, as well as the successful immobilization of GOx on the surface of the pristine and Ag-doped ZnO nanosheets (ESI,† section S2.1).

4. Electrochemical analysis of electrodes

Electrochemical impedance spectroscopy (EIS) was performed to study the electron transfer properties between the electrode surface and electrolyte. Fig. 5(a) shows the Nyquist plots for the pristine ZnO and Ag-doped ZnO electrodes prepared on ITO substrates. The resulting data were then fitted to an equivalent electrical circuit (EEC) that provides quantitative information regarding the processes happening at the electrode surface. Here, the observed data were fitted to a Randles equivalent circuit model as shown in Fig. 5(a) (inset), where R_s, C_{dl}, R_{ct}, and Z_w correspond to the solution (or ionic) resistance of the electrolyte, double layer capacitance, charge-transfer resistance, and Warburg resistance, respectively. As listed in Table S2 (ESI†), the decreasing value of R_{ct} revealed the enhancement of electron transfer between the solution and the electrodes, suggesting that doping may enhance the charge transfer ability of ZnO.[65]

Further, as presented in Fig. 5(b), cyclic voltammograms (CVs) of the pristine and Ag-doped ZnO electrodes prepared on ITO substrates were recorded at a scan rate (v) of 10 mV s^{-1}. The CVs revealed that the anodic (oxidation) and cathodic (reduction) peak currents of the electrodes are at ~0.32 V and ~0.14 V, respectively. Also, it was observed that the magnitude of the anodic and cathodic peak currents increases as the concentration of the Ag dopant increases in the ZnO host matrix, reaching a maximum value of ~0.541 mA and ~0.492 mA, respectively, for the ZnO:Ag5/ITO electrode. Here, the introduction of defect states by Ag doping in the ZnO host matrix (EDX & XPS results) and the improved surface area (SEM results) are the two main factors responsible for the rapid charge transfer rate between the electrode and the electrolyte, resulting in an enhancement in the electrochemical response of the electrodes.[66] Next, CV measurements were also performed at different scan rates (v = 10, 20, 40, 60, 80, and 100 mV s^{-1}) to investigate the kinetics and transfer characteristics of the prepared pristine and Ag-doped ZnO electrodes (ESI,† Fig. S4(a–f)). From Fig. S4(a–f),† it was observed that the anodic peak current (I_{pa}) and cathodic peak current (I_{pc}) are shifted towards positive and negative potentials, respectively, with increasing scan rate. Also, the ratio of peak currents (*i.e.*, anodic to cathodic) for all the electrodes (Table S3†) was found to be larger than unity. These results suggest that the pristine and Ag-doped ZnO electrodes have a quasi-reversible nature.[67,68] As shown in Fig. S5(a–f), it was observed that I_{pa} and I_{pc} for all the electrodes increase linearly with the scan rate and the square root of the scan rate, respectively, indicating that the electrodes undergo a combination of surface and diffusion controlled electrochemical processes.[69] The diffusion coefficient (D) of redox species from the electrolyte to electrodes and the surface concentration of electroactive sites (I^*) were calculated using the Randles–Sevcik equation, I_{pa} = $(2.69 \times 10^5)A_e D^{1/2} n^{3/2} v^{1/2} C$, and Brown Anson model, I_{pa} =

Table 1 Comparison of the current work with previously reported enzymatic and non-enzymatic glucose sensing electrodes based on pristine and doped-ZnO nanostructures

Method used	Sensing electrode		Sensitivity (μA mM^{-1} cm^{-2})	Linear range (mM)	Response time (s)	K_m^{app} (mM)	Ref.
	Enzymatic	Non-enzymatic					
Electrochemical	GOx/ZnO:Co	—	13.3	0–4	8	21	79
	GOx/porous ZnO	—	23.4	0.1–1	7	—	80
	GOx/ZnO-NWs/graphite	—	13–17	—	—	2.11	81
	GOx/ZnO Nanorod array	—	18.7	0.5–2.5	<5	1.3	82
	GOx/ZnO–Al	—	5.5	0.28–28	10	66.7	83
	GOx/ZnO–Ag	—	3.85	1.5×10^{-3}–6.5	—	3.87	21
	GOx/ZnO$_{(Co–Fe)}$/ITO	—	32.2	0–4	6.21	0.054	84
		ZnO/MWCNT/GCE	64.29	—	—	—	12
		ZnO/Ti	7.65	3.33–11.1	—	—	85
	GOx/ZnO:Ag5/ITO	—	~98.3	0–4	~5	~0.26	This work
		ZnO:Ag5/ITO	~104.7	0–3	~5	—	This work

Method used	Sensing electrode		Sensitivity (% mM^{-1})	Linear range (mM)	Response time (s)	K_m^{app} (mM)	Ref.
	Enzymatic	Non-enzymatic					
Fluorescence spectroscopy	—	ZnO nanotubes	3.5	0.1–15	—	—	86
	—	ZnO nanorods	1.4	0.5–30	—	—	87
	Gox/ZnO nanoparticles	—	0.5	10–130	—	—	88

Method used	Sensing electrode						
	Enzymatic	Non-enzymatic	Sensitivity	Linear range	Response time	K_m^{app}	Ref.
Surface plasmon resonance	GOx/ZnO/Au/prism	—	—	0–300 mg dl^{-1}	—	—	89
Surface enhanced Raman spectroscopy	GOx/CdSe/ ZnS QDs decorated ZnO NRs	—	—	0.03–3 mM	—	—	90

$n^2F^2vAI*/4RT$, respectively,[70,71] where I_{pa}, A_e, n, v, C, F, R, and T, are the anodic peak current, geometrical surface area of the electrode, number of electrons transferred, scan rate, redox species concentration, Faraday constant, universal gas constant, and absolute temperature, respectively. Further, using the calculated D and Randles–Sevcik equation, the electroactive surface area (A_e) of all the electrodes was calculated (ESI,† Table S3), and found that Ag-doped ZnO electrodes provide increased electroactive surface area for the loading of enzymes than that of pristine ZnO electrodes. According to Hrapovic et al.,[72] nanomaterials with a larger electroactive surface area have higher electrocatalytic activity, resulting in increased sensitivity.

Furthermore, as shown in Fig. 6(A)(a)–(c), it was observed that the magnitude of the peak current significantly decreases when GOx is immobilized onto the surface of the ZnO/ITO, ZnO:Ag2/ITO, and ZnO:Ag5/ITO electrodes. This is because of the insulating nature of the GOx layer, which acts as a barrier between the electrode surface and the redox species in the buffer solution, limiting charge transfer.[73] In addition, CV measurements were also performed at different scan rates for the GOx/ZnO/ITO, GOx/ZnO:Ag2/ITO, and GOx/ZnO:Ag5/ITO samples (ESI,† Fig. S4(g–i)), indicating the quasi-reversible nature of the GOx immobilized electrodes. As listed in Table S3 (ESI†), it can be seen that the calculated values of the surface concentration of the GOx/ZnO/ITO, GOx/ZnO:Ag2/ITO and GOx/ZnO:Ag5/ITO electrodes differ from those of the ZnO/ITO, ZnO:Ag2/ITO, and ZnO:Ag5/ITO

electrodes. All these results confirm the successful immobilization of GOx onto the surface of the ZnO/ITO, ZnO:Ag2/ITO, and ZnO:Ag5/ITO samples,[72,73] which is also supported by the FTIR results (Fig. S3†).

5. Sensing measurements

Electrochemical sensors are an important subclass of chemical sensors in which an electrode is used as a transduction element. It works on the principle that an electrical current passes through a sensing electrode, which is produced by an electrochemical reaction that takes place at the electrode's surface.[74] In the present work, we have investigated the electrochemical response of both prepared enzymatic and non-enzymatic electrodes for glucose sensing.

5.1 Enzymatic glucose sensing

Fig. 6(B)(a)–(c) show the CVs of the fabricated GOx/ZnO/ITO, GOx/ZnO:Ag2/ITO and GOx/ZnO:Ag5/ITO sensing electrodes in the presence of a glucose concentration of 0–8 mM. It was observed that the response current increases with increasing glucose concentration (corresponding inset of Fig. 6(B)), and saturates beyond a glucose concentration of 3 mM, 3 mM, and 4 mM for the GOx/ZnO/ITO, GOx/ZnO:Ag2/ITO and GOx/ZnO:Ag5/ITO sensing electrodes, respectively. The sensitivity and the LOD of the fabricated electrodes were calculated using eqn (S.1) and (S.2),† respectively, and are described in Table S3 (ESI†). It was observed that the GOx/ZnO:Ag5/ITO
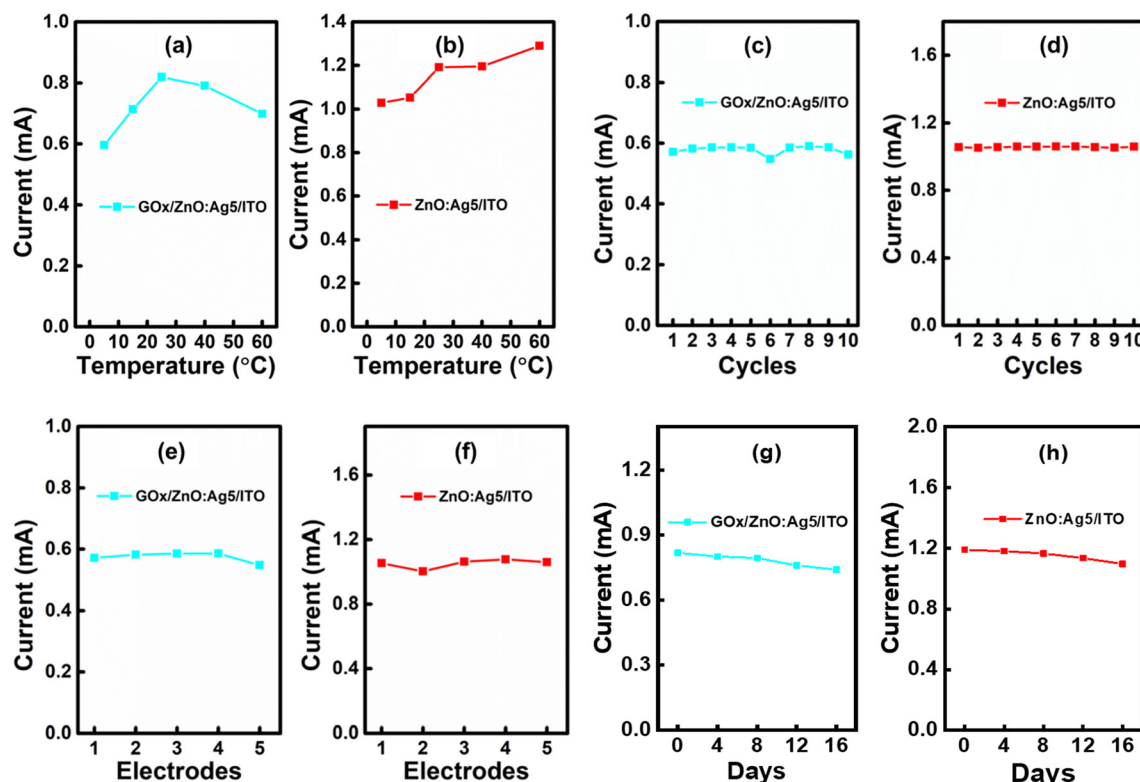
Fig. 8 Effect of temperature on the fabricated (a) enzymatic (GOx/ZnO:Ag5/ITO) and (b) non-enzymatic (ZnO:Ag5/ITO) sensing electrodes at 1 mM glucose concentration. Current response of the (c) enzymatic (GOx/ZnO:Ag5/ITO) and (d) non-enzymatic (ZnO:Ag5/ITO) sensing electrodes for 10 cycles at 1 mM glucose concentration. Current response of the (e) enzymatic (GOx/ZnO:Ag5/ITO) and (f) non-enzymatic (ZnO:Ag5/ITO) sensing electrodes for 5 different electrodes at 1 mM glucose concentration. Current response of the (g) enzymatic (GOx/ZnO:Ag5/ITO) and (h) non-enzymatic (ZnO:Ag5/ITO) sensing electrodes at 1 mM glucose concentration over 16 days.

electrode exhibits excellent glucose-sensing characteristics (high sensitivity $\sim$98.3 μA mM^{-1} cm^{-2} and low LOD $\sim$0.098 mM) compared to the GOx/ZnO:Ag2/ITO (sensitivity $\sim$15.3 μA mM^{-1} cm^{-2} and LOD $\sim$0.451 mM) and GOx/ZnO/ITO (sensitivity $\sim$37.5 μA mM^{-1} cm^{-2} and LOD $\sim$0.204 mM) electrodes. The reason for the higher achieved sensitivity and lower LOD for the sample GOx/ZnO:Ag5/ITO is the incorporation of an optimum amount of Ag ions in the ZnO host matrix, resulting in a rapid electron transfer rate between the sensing electrode surface and electrochemically active species, as well as the improved catalytic character of GOx towards glucose.[36] Further, the apparent Michaelis–Menten constant (K_m^{app}) was calculated to examine the biological activity of immobilized GOx using the Lineweaver–Burk relation (eqn (1)),[75] where I_{pa}, $I_{pa(max)}$, and C_g are the anodic current, maximum anodic current, and concentration of glucose, respectively.

$$1/I_{pa} = (K_m^{app}/I_{pa(max)})(1/C_g) + 1/I_{pa(max)} \qquad (1)$$

The value of K_m^{app} for the GOx/ZnO/ITO, GOx/ZnO:Ag2/ITO, and GOx/ZnO:Ag5/ITO sensing electrodes was estimated to be $\sim$0.07, $\sim$0.04 and $\sim$0.26 mM, respectively. A smaller K_m^{app} value indicates that the immobilized GOx has high enzymatic activity, and thus has a higher affinity for glucose for the fabricated sensing electrodes.[76] However, enzymatic biosensors are unstable (influenced by a variety of parameters such as temperature, pH, etc.) and quite expensive.[77,78] Therefore, in this work, we have also fabricated non-enzymatic electrodes based on the Ag-doped ZnO nanosheets for glucose sensing.

5.2 Non-enzymatic glucose sensing

In this study, our objective was to develop a non-enzymatic glucose sensor, which was evaluated based on the performance of Electrochemical Impedance Spectroscopy (EIS) (refer to Fig. 5(a)) and Cyclic Voltammetry (CV) (refer to Fig. 5(b)) for all the samples. With results shown in Fig. 5(a) and (b), it was observed that the 5% Ag-doped ZnO nanosheets (ZnO:Ag5/ITO) displayed excellent electrochemical characteristics, which is favorable for designing non-enzymatic glucose sensors. Thus, as presented in Fig. 7(A), we have fabricated a non-enzymatic electrode based on ZnO:Ag5/ITO and studied its glucose-sensing performance in the concentration range of 0–8 mM. The fabricated non-enzymatic electrode exhibited a higher sensitivity of $\sim$104.7 μA mM^{-1} cm^{-2} and good linearity of $\sim$0.981, with a lower LOD of $\sim$0.06 mM, in comparison to the enzymatic biosensor (GOx/ZnO:Ag5/ITO, sensitivity $\sim$98.3 μA mM^{-1} cm^{-2}, LOD $\sim$0.098 mM and linearity $\sim$0.92). Moreover, as listed in Table 1, we have compared our fabricated glucose sensors based
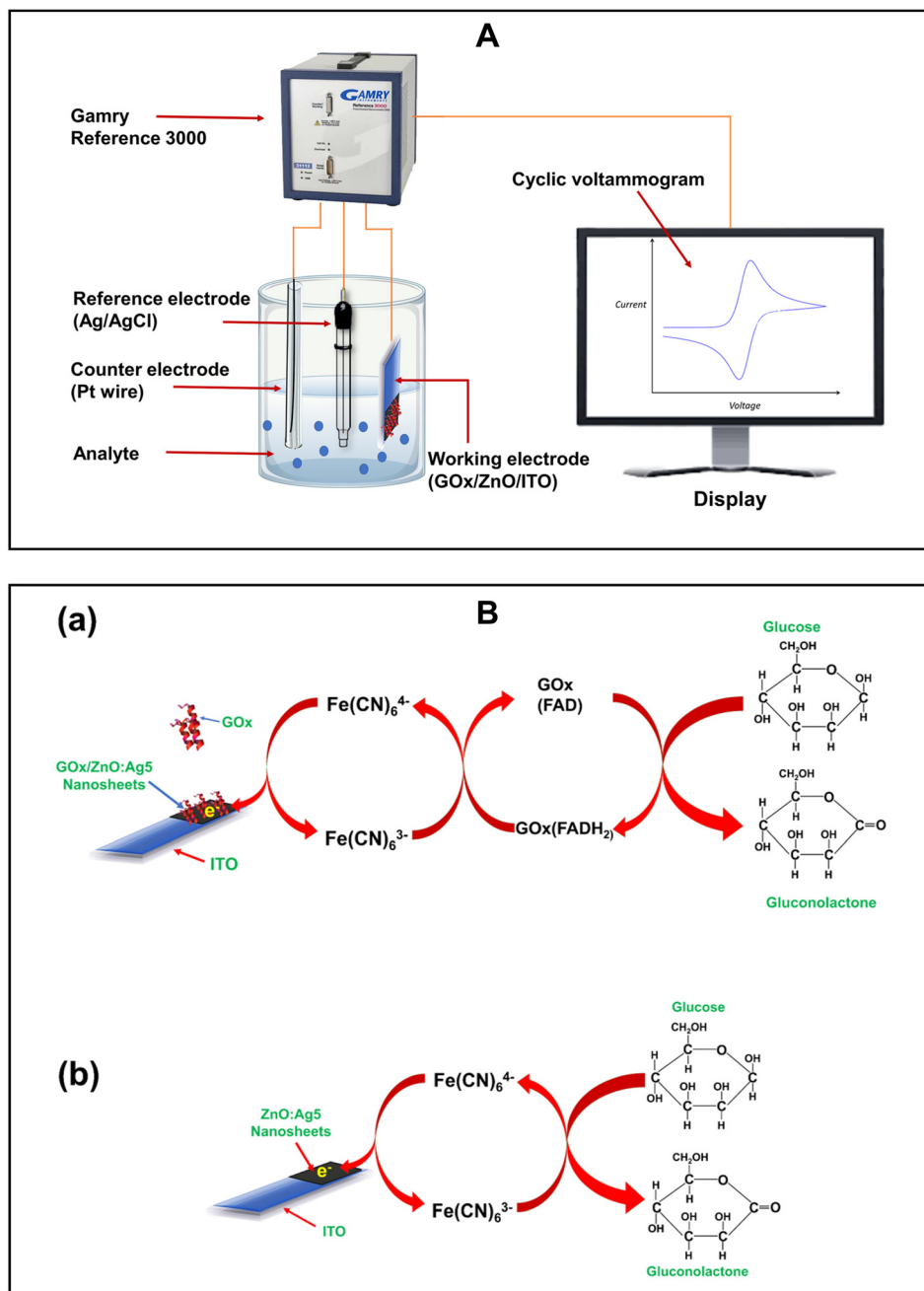
Fig. 9 A. Schematic of the electrochemical (CV) analysis using an electrochemical workstation. B. The schematic representations of the electrochemical oxidation of glucose for the (a) enzymatic (GOx/ZnO:Ag5/ITO) and (b) non-enzymatic (ZnO:Ag5/ITO) sensing electrodes.

on Ag-doped ZnO nanosheets with previously reported glucose sensors based on pristine and doped-ZnO nanostructures.

Furthermore, anti-interference ability (selectivity), the effect of temperature, repeatability, and reproducibility are important aspects for the practical application of fabricated sensing electrodes (ESI† Fig. S6 and S7). It is well known that a few electro-active species such as dopamine, cholesterol, ascorbic acid, uric acid, cysteine, *etc.* in serum may affect the performance of a biosensor.[91] Thus, the anti-interference capability and selectivity of the prepared biosensor have been studied by introducing electro-active species: uric acid (UA),

cholesterol (Chol.), and ascorbic acid (AA). Fig. 7(B) shows the anti-interference ability of the fabricated enzymatic and non-enzymatic sensing electrodes based on ZnO:Ag5 nanosheets. Selectivity measurements were performed with the addition of the interfering species 0.5 mM UA, 0.5 mM Chol., and 0.5 mM AA to a standard solution of 1 mM glucose concentration. As shown in Fig. 7(B)(a), although the interfering species slightly increased the current response, these results can be ruled out, as the highest concentration of these interfering species in the human body is approximately 0.1 mM.[68,92] Consequently, the sensing

electrodes can be used to determine glucose levels in human serum samples under physiological conditions. As presented in Fig. 7(B)(b), the ZnO:Ag5 nanosheet based enzymatic and non-enzymatic sensing electrodes exhibited a current response of ~20.2% (1 mM glucose), ~1.7% (0.5 mM UA), ~0.16% (0.5 mM Chol.), and ~7.9% (0.5 mM AA), and ~20.4% (1 mM glucose), ~4.05% (for 0.5 mM UA), 1.11% (for 0.5 mM Chol.), and 6.4% (for 0.5 mM AA), respectively. These results show that both the enzymatic and non-enzymatic sensing electrodes based on the ZnO:Ag5 nanosheets are highly selective towards glucose; however, the non-enzymatic sensing electrode has better selectivity towards glucose as compared to the enzymatic electrode.

Fig. 8(a) and (b) show the effect of temperature (5 °C to 60 °C) on both enzymatic and non-enzymatic sensing electrodes. It is found that the non-enzymatic sensing electrode exhibited a small change in current response (~0.25–13%) with temperature compared to the enzymatic sensing electrode (~0.12–28%), indicating that the non-enzymatic glucose sensing electrode has better temperature stability in comparison to the enzymatic glucose sensing electrode. As presented in Fig. 8(c) and (d), the repeatability of the both prepared enzymatic and non-enzymatic electrodes was determined by analyzing the current response in 1 mM glucose 10 times in a single day (ESI† Fig. S5(a and b)). The relative standard deviation (RSD) was calculated for the 10 repeated cycles and was found to be 2.4% and 0.3% for the enzymatic and non-enzymatic sensing electrodes, respectively, revealing the excellent repeatability of the fabricated electrodes. Likewise, as shown in Fig. 8(e) and (f), we have also investigated the reproducibility of both enzymatic and non-enzymatic sensing electrodes which was examined by analyzing the current response in 1 mM glucose for five distinct electrodes (ESI† Fig. S5(c and d)). The calculated RSD values for both enzymatic and non-enzymatic sensing electrodes were found to be ~1.9% and ~1.8%, respectively, suggesting good reproducibility. Besides, it can be seen from Fig. 8(c–f) that the fabricated non-enzymatic glucose sensing electrode has better repeatability and reproducibility than the enzymatic glucose sensing electrode. Next, the stability of both electrodes was tested by measuring the current response in 1 mM glucose for 16 days. When not in use, the modified enzymatic electrode was kept dry at 4 °C and the non-enzymatic electrode was kept in a desiccator. As shown in Fig. 8(g) and (h), the prepared enzymatic glucose sensing electrode maintained 97% of its original response after 8 days and 90.5% after 16 days, and the non-enzymatic glucose sensing electrode maintained 98% of its initial response after 8 days and 92% after 16 days, suggesting high storage stability.

6. Mechanism of glucose sensing

Fig. 9A shows a schematic diagram of CV analysis of the prepared electrodes for glucose monitoring using an electrochemical workstation. Schematic representations of

the electrochemical oxidation of glucose on the ZnO:Ag5 nanosheet based ITO electrode surface for enzymatic and non-enzymatic glucose sensing are shown in Fig. 9B(a) and (b), respectively. The electrochemical recognition of glucose was performed using $Fe[(CN)_6]^{3-/4-}$ as a redox mediator to avoid electrode contamination and improve redox cycling.[90] As presented in Fig. 9B(a), immobilized GOx on the ZnO:Ag5 nanosheet-based electrode oxidizes glucose to gluconolactone while simultaneously converting from GOx(FAD) into GOx(FADH_2). Then, the redox mediator $Fe[(CN)_6]^{3-}$ reacts with the reduced GOx and accepts electrons to become electro-reduced $Fe[(CN)_6]^{4-}$ and regenerates the oxidized GOx. Further, these electrons are transported from $Fe[(CN)_6]^{4-}$ to ZnO:Ag5 nanosheets and eventually to the ITO electrode.[93–96] An oxidation current is generated when $Fe[(CN)_6]^{4-}$ returns to its oxidized state $Fe[(CN)_6]^{3-}$. Next, the probable mechanism of glucose oxidation on the ZnO:Ag5 nanosheet surface for the application of a non-enzymatic glucose sensor is depicted in Fig. 9B(b). At first, glucose is oxidized to gluconolactone by releasing electrons, and then the redox mediator $Fe[(CN)_6]^{3-}$ accepts these electrons and becomes $Fe[(CN)_6]^{4-}$. Further, these electrons transfer to the nanosheets, resulting in an oxidation current.[95,97] Thus, the current response obtained in the presence of glucose (Fig. 6(B) and 7(A)) is caused by these released electrons for both enzymatic and non-enzymatic glucose sensing.

7. Conclusions

In summary, pristine and Ag-doped ZnO nanosheets were successfully synthesized by a hydrothermal method and it was found that Ag doping improved the electrochemical characteristics of the ZnO matrix, which has a significant impact on the glucose-sensing performance with and without the enzyme GOx. FESEM images revealed the growth of nanosheet-like morphologies in pristine and Ag-doped ZnO samples and it was also observed that the grain size and thickness decrease with increasing Ag-dopant concentration in the ZnO host matrix. The XRD, EDX, XPS, and FTIR results showed the formation of pristine ZnO and successful incorporation of Ag dopants into the ZnO matrix, including the presence of different defect sites in the samples. Further, FTIR spectra revealed the successful immobilization of GOx on the surface of the pristine ZnO and Ag-doped ZnO samples. For application as glucose sensors, the pristine and Ag-doped ZnO-based ITO electrodes are studied electrochemically. Among all prepared electrodes, the 5% Ag-doped ZnO nanosheet electrode showed a higher conductivity than the pristine and other Ag-doped ZnO electrodes, which may be due to the introduction of defect states by Ag doping in the ZnO host matrix as well as the improved surface area. At room temperature, for non-enzymatic glucose sensing, the 5% Ag-doped ZnO nanosheet electrode exhibited higher sensitivity (~104.7 μA mM^{-1} cm^{-2}), lower detection limits (~0.06 mM), good linearity (~0.981), higher selectivity,

reasonable repeatability, and good reproducibility and stability compared to that for enzymatic glucose sensing (sensitivity ~ 98.3 μA mM^{-1} cm^{-2}, LOD ~ 0.098 mM and linearity ~ 0.92). We demonstrate a high sensing performance without using any enzyme on Ag-doped ZnO nanosheets fabricated *via* a simple approach which may be a potential candidate for low-cost biosensors and could have a wide range of applications in clinical diagnosis, industry, and food science.

Conflicts of interest

The authors declare that they have no known competing financial interests or personal relationships that could have appeared to influence the work reported in this paper.

Acknowledgements

References

1 E. E. Ventura, J. N. Davis and M. I. Goran, *Obesity*, 2011, **19**(4), 868–874.

2 F. Conzuelo, M. Gamella, S. Campuzano, M. A. Ruiz, A. J. Reviejo and J. M. Pingarron, *J. Agric. Food Chem.*, 2010, **58**(12), 7141–7148.

3 V. Scognamiglio, *Biosens. Bioelectron.*, 2013, **47**, 12–25.

4 N. S. Ridhuan, K. A. Razak and Z. Lockman, *Sci. Rep.*, 2018, **8**(1), 1–12.

5 P. Hu, R. Zhou, D. Wang, H. Luo, X. Xiong, K. Huang, L. Li and P. Chen, *Sens. Actuators, B*, 2020, **308**, 127702.

6 B. Liu, Z. Sun, P. J. Huang and J. Liu, *J. Am. Chem. Soc.*, 2015, **137**, 1290–1295.

7 H. He, X. Xu, H. Wu and Y. Jin, *Adv. Mater.*, 2012, **24**(13), 1736–1740.

8 H. Teymourian, A. Barfidokht and J. Wang, *Chem. Soc. Rev.*, 2020, **49**(21), 7671–7709.

9 A. Heller and B. Feldman, *Chem. Rev.*, 2008, **108**(7), 2482–2505.

10 A. Wei, X. W. Sun, J. X. Wang, Y. Lei, X. P. Cai, C. M. Li and W. Huang, *Appl. Phys. Lett.*, 2006, **89**(12), 123902.

11 T. Kong, Y. Chen, Y. Ye, K. Zhang, Z. Wang and X. Wang, *Sens. Actuators, B*, 2009, **38**(1), 344–350.

12 S. M. U. Ali, O. Nur, M. Willander and B. Danielsson, *Sens. Actuators, B*, 2010, **145**(2), 869–874.

13 C. L. Hsu, J. H. Lin, D. X. Hsu, S. H. Wang, S. Y. Lin and T. J. Hsueh, *Sens. Actuators, B*, 2017, **238**, 150–159.

14 Z. Wang, J. Zhang, R. Jian, J. Liao, X. Xiong and K. Huang, *Microchem. J.*, 2020, **159**, 105396.

15 S. D. Lawaniya, S. Kumar, Y. Yu, H. G. Rubahn, Y. K. Mishra and K. Awasthi, *Mater. Today Chem.*, 2023, **29**, 101428.

16 N. Tripathy and D. H. Kim, Metal oxide modified ZnO nanomaterials for biosensor applications, *Nano Convergence*, 2018, **5**(1), 1–10.

17 A. Tereshchenko, M. Bechelany, R. Viter, V. Khranovskyy, V. Smyntyna, N. Starodub and R. Yakimova, *Sens. Actuators, B*, 2016, **229**, 664–677.

18 L. Cao, J. Kiely, M. Piano and R. Luxton, *Sci. Rep.*, 2018, **8**(1), 1–9.

19 N. R. Shanmugam, S. Muthukumar and S. Prasad, *Future Sci. OA*, 2017, **3**(4), FSO196.

20 J. Li, S. Ma, X. Liu, Z. Zhou and C. Q. Sun, *Chem. Rev.*, 2012, **112**(5), 2833–2852.

21 B. Ortiz-Casas, A. Galdámez-Martínez, J. Gutiérrez-Flores, A. B. Ibañez, P. K. Panda, G. Santana and A. Dutt, *Mater. Today*, 2021, **50**, 533–569.

22 Z. L. Wang, *Mater. Today*, 2004, **7**(6), 26–33.

23 N. Izyumskaya, V. Avrutin, Ü. Özgür, Y. I. Alivov and H. Morkoç, *Phys. Status Solidi B*, 2007, **244**(5), 1439–1450.

24 A. Mahmoud, M. Echabaane, K. Omri, J. Boudon, L. Saviot, N. Millot and R. B. Chaabane, *Molecules*, 2021, **26**(4), 929.

25 W. Raza and K. Ahmad, *Mater. Lett.*, 2018, **212**, 231–234.

26 J. Luo, P. Luo, M. Xie, K. Du, B. Zhao, F. Pan and G. Liang, *Biosens. Bioelectron.*, 2013, **49**, 512–518.

27 M. Shukla, J. Agrawal, T. Dixit, I. A. Palani and V. Singh, *Mater. Res. Express*, 2018, **5**(5), 055031.

28 J. Ghosh, R. Ghosh and P. K. Giri, *Sens. Actuators, B*, 2018, **254**, 681–689.

29 G. Vijayaprasath, R. Murugan, J. S. Narayanan, V. Dharuman, G. Ravi and Y. Hayakawa, *J. Mater. Sci.: Mater. Electron.*, 2015, **26**(7), 4988–4996.

30 A. Mahmoud, M. Echabaane, K. Omri, L. El Mir and R. B. Chaabane, *J. Alloys Compd.*, 2019, **786**, 960–968.

31 W. C. Peng, Z. H. Wang, C. C. Yang, C. S. Huang, Y. K. Su and J. L. Ruan, in *SPIE Proc. Biomed. Imag. Sens. Conf.*, 2017, vol. 10251, pp. 165–167.

32 P. Chakraborty, T. Majumder, S. Dhar and S. P. Mondal, *AIP Conf. Proc.*, 2018, **1942**, 050074.

33 S. S. Patil, M. G. Mali, M. S. Tamboli, D. R. Patil, M. V. Kulkarni, H. Yoon, H. Kim, S. S. Al-Deyab, S. S. Yoon, S. S. Kolekar and B. B. Kale, *Catal. Today*, 2016, **260**, 126–134.

34 Y. Zheng, L. Zheng, Y. Zhan, X. Lin, Q. Zheng and K. Wei, *Inorg. Chem.*, 2007, **46**, 6980–6986.

35 F. Xian, K. Miao, X. Bai, Y. Ji, F. Chen and X. Li, *Optik*, 2013, **124**, 4876–4879.

36 F. Zhou, W. Jing, P. Liu, D. Han, Z. Jiang and Z. Wei, *Sensors*, 2017, **17**(10), 2214.

37 J. Jaiswal, A. Sanger, P. Tiwari and R. Chandra, *Sens. Actuators, B*, 2020, **305**, 127437.

38 C. Li, Y. Lin, F. Li, L. Zhu, D. Sun, L. Shen and S. Ruan, *RSC Adv.*, 2015, **5**(98), 80561–80567.

39 X. Pan, X. Liu, A. Bermak and Z. Fan, *ACS Nano*, 2013, **7**(10), 9318–9324.

40 A. Fulati, S. M. U. Ali, M. H. Asif, M. Willander, C. Brännmark, P. Strålfors and B. Danielsson, *Sens. Actuators, B*, 2010, **150**(2), 673–680.

41 N. Akhtar, S. K. Metkar, A. Girigoswami and K. Girigoswami, *Mater. Sci. Eng., C*, 2017, **78**, 960–968.

42 H. M. Kim, J. H. Park and S. K. Lee, *Sci. Rep.*, 2019, **9**(1), 1–9.

43 F. Zhang, X. Wang, S. Ai, Z. Sun, Q. Wan, Z. Zhu and K. Yamamoto, *Anal. Chim. Acta*, 2004, **519**(2), 155–160.

44 M. Liu, P. Song, D. Liang, Z. Yang and Q. Wang, *Mater. Res. Express*, 2019, **6**(12), 125910.

45 J. Jaiswal, A. Das, V. Chetry, S. Kumar and R. Chandra, *Sens. Actuators, B*, 2022, **359**, 131552.

46 S. K. Arya, S. Saha, J. E. Ramirez-Vick, V. Gupta, S. Bhansali and S. P. Singh, *Anal. Chim. Acta*, 2012, **737**, 1–21.

47 N. Baig, I. Kammakakam and W. Falath, *Mater. Adv.*, 2021, **2**(6), 1821–1871.

48 E. Andrade and M. Miki-Yoshida, *Thin Solid Films*, 1999, **350**(1–2), 192–202.

49 A. Kołodziejczak-Radzimska and T. Jesionowski, *Materials*, 2014, **7**(4), 2833–2881.

50 K. S. Babu and V. Narayanan, *Chem. Sci. Trans.*, 2013, **2**(S1), S33–S36.

51 S. A. Kaur, G. S. Randhawa and R. Singh, *IOSR J. Appl. Phys.*, 2017, **9**, 18–24.

52 R. S. Zeferino, M. B. Flores and U. Pal, *J. Appl. Phys.*, 2011, **109**(1), 014308.

53 S. Khosravi-Gandomani, R. Yousefi, F. Jamali-Sheini and N. M. Huang, *Ceram. Int.*, 2014, **40**(6), 7957–7963.

54 B. D. Ahn, H. S. Kang, J. H. Kim, G. H. Kim, H. W. Chang and S. Y. Lee, *J. Appl. Phys.*, 2006, **100**(9), 093701.

55 C. Karunakaran, V. Rajeswari and P. Gomathisankar, *Superlattices Microstruct.*, 2011, **50**(3), 234–241.

56 J. Jaiswal, P. Tiwari, P. Singh and R. Chandra, *Sens. Actuators, B*, 2020, **325**, 128800.

57 S. K. Pandey, S. K. Pandey, C. Mukherjee, P. Mishra, M. Gupta, S. R. Barman and S. Mukherjee, *J. Mater. Sci.: Mater. Electron.*, 2013, **24**(7), 2541–2547.

58 A. Meng, S. Sun, Z. Li and J. Han, *Adv. Powder Technol.*, 2013, **24**(1), 224–228.

59 S. M. Hosseini, I. A. Sarsari, P. Kameli and H. Salamati, *J. Alloys Compd.*, 2015, **640**, 408–415.

60 J. Jaiswal, P. Singh and R. Chandra, *Sens. Actuators, B*, 2021, **327**, 128862.

61 S. Gandla, S. R. Gollu, R. Sharma, V. Sarangi and D. Gupta, *Appl. Phys. Lett.*, 2015, **107**(15), 152102.

62 K. M. Wong, Y. Fang, A. Devaux, L. Wen, J. Huang, L. De Cola and Y. Lei, *Nanoscale*, 2011, **3**(11), 4830–4839.

63 L. Jing, Z. Xu, J. Shang, X. Sun, W. Cai and H. Guo, *Mater. Sci. Eng., A*, 2002, **332**, 356–361.

64 I. Ahmad, E. Ahmad and M. Ahmad, *SN Appl. Sci.*, 2019, **1**(4), 1–12.

65 M. Karyaoui, D. B. Ahmed, M. Jemia, I. B. Gannouni, A. Assaker, M. Amlouk Bardaoui and R. Chtourou, *Inorg. Chem. Commun.*, 2020, **119**, 108114.

66 K. Jindal, M. Tomar and V. Gupta, *Analyst*, 2013, **138**(15), 4353–4362.

67 E. A. Gomaa, A. Negm and R. M. Abu-Qarn, *Measurement*, 2018, **125**, 645–650.

68 N. S. Ridhuan, K. A. Razak and Z. Lockman, *Sci. Rep.*, 2018, **8**(1), 1–12.

69 L. Fotouhi, M. Fatollahzadeh and M. M. Heravi, *Int. J. Electrochem. Sci.*, 2012, **7**, 3919–3928.

70 A. J. Bard, L. R. Faulkner and H. S. White, *Electrochemical methods: Fundamentals and applications*, John Wiley & Sons, 2022.

71 A. Sharma, D. Baral, H. B. Bohidar and P. R. Solanki, *Chem.-Biol. Interact.*, 2015, **238**, 129–137.

72 S. Hrapovic, Y. Liu, K. B. Male and J. H. T. Luong, *Anal. Chem.*, 2004, **76**(4), 1083–1088.

73 A. Sharma, K. Rawat, P. R. Solanki and H. B. Bohidar, *Anal. Methods*, 2015, **7**(14), 5876–5885.

74 F. R. Simões and M. G. Xavier, *Nanosci. and its Appl.*, 2017, vol. 1, pp. 155–178.

75 R. Ahmad, N. Tripathy, J. H. Kim and Y. B. Hahn, *Sens. Actuators, B*, 2012, **174**, 195–201.

76 J. R. Li, Y. K. Du, P. Boullanger and L. Jiang, *Thin Solid Films*, 1999, **352**(1–2), 213–217.

77 L. Alvarado-Ramírez, M. Rostro-Alanis, J. Rodríguez-Rodríguez, J. E. Sosa-Hernández, E. M. Melchor-Martínez, H. Iqbal and R. Parra-Saldívar, *Biosensors*, 2021, **11**(11), 410.

78 V. Naresh and N. Lee, *Sensors*, 2021, **21**(4), 1109.

79 Z. W. Zhao, X. J. Chen, B. K. Tay, J. S. Chen, Z. J. Han and K. A. Khor, *Biosens. Bioelectron.*, 2007, **23**(1), 135–139.

80 H. Fatemi, A. A. Khodadadi, A. A. Firooz and Y. Mortazavi, *Curr. Appl. Phys.*, 2012, **12**(4), 1033–1038.

81 P. Gallay, E. Tosi, R. Madrid, M. Tirado and D. Comedi, *Nanotechnology*, 2016, **27**(42), 425501.

82 M. Shukla, T. Dixit, R. Prakash, I. A. Palani and V. Singh, *Appl. Surf. Sci.*, 2017, **422**, 798–808.

83 V. T. K. P. Fidal, S. Inguva, S. Krishnamurthy, E. Marsili, J. P. Mosnier and T. S. Chandra, *Enzyme Microb. Technol.*, 2017, **96**, 67–74.

84 S. Baruah, B. Maibam, C. K. Borah, T. Agarkar, A. Kumar and S. Kumar, *IEEE Sens. J.*, 2021, **21**(13), 14601–14608.

85 G. Villasana-Ponce, F. Chalé-Lara, J. Olarte Villamizar, M. Zapata-Torres, E. Valaguez Velázquez, N. Cruz González and A. Márquez Herrera, *Superficies Vacio*, 2019, **32**, 22–26.

86 H. H. Mai, D. H. Tran and E. Janssens, *Microchim. Acta*, 2019, **186**, 1–10.

87 S. N. Sarangi, S. Nozaki and S. N. Sahu, *J. Biomed. Nanotechnol.*, 2015, **11**(6), 988–996.

88 D. Sodzel, V. Khranovskyy, V. Beni, A. P. Turner, R. Viter, M. O. Eriksson and R. Yakimova, *Microchim. Acta*, 2015, **182**, 1819–1826.

89 A. Paliwal, R. Gaur, A. Sharma, M. Tomar and V. Gupta, *Optik*, 2016, **127**(19), 7642–7647.

90 L. Chen, W. H. Tse, Y. Chen, M. W. Melling, J. McDonald and J. Zhang, *Biosens. Bioelectron.*, 2017, **91**, 393–399.

91 R. Sha, A. Basak, P. C. Maity and S. Badhulika, *Sens. Actuators Rep.*, 2022, **4**, 100098.

92 G. Aydoğdu, D. K. Zeybek, Ş. Pekyardımcı and E. Kılıç, *Artif. Cells, Nanomed., Biotechnol.*, 2013, **41**(5), 332–338.

93 D. Sharma, Y. Lim, Y. Lee and H. Shin, *Anal. Chim. Acta*, 2015, **88**, 194–202.

94 S. H. Lee, H. Y. Fang, W. C. Chen, H. M. Lin and C. A. Chang, *Anal. Bioanal. Chem.*, 2005, **383**(3), 532–538.

95 H. Deng, A. K. L. Teo and Z. Gao, *Sens. Actuators, B*, 2014, **191**, 522–528.

96 K. Tian, S. Alex, G. Siegel and A. Tiwari, *Mater. Sci. Eng., C*, 2015, **46**, 548–552.

97 A. Senthamizhan, B. Balusamy and T. Uyar, *Anal. Bioanal. Chem.*, 2016, **408**(5), 1285–1306.